SECONDARY KELVIN-HELMHOLTZ INSTABILITY IN A STABLY STRATIFIED TEMPORAL MIXING LAYER

Denise Maria Varella Martinez
FURG - Departamento de Matemática
Programa de Pós Graduação em Recursos Hídricos e Saneamento Ambiental- IPH - UFRGS
Av. Bento Gonçalves 9500, RS - 90650 001, Brazil
denisevmartinez@yahoo.com.br

Edith Beatriz Camaño Schettini
UFRGS - Instituto de Pesquisas Hidráulicas
Av. Bento Gonçalves, 9500 Porto Alegre, RS - 906500 001, Brazil
bcamano@iph.ufrgs.br

Jorge Hugo Silvestrini
PUCRS - Pontifícia Universidade Católica do Rio Grande do Sul
Departamento de Engenharia Mecânica e Mecatrônica
Av. Ipiranga , 6681- Porto Alegre - RS - 90619-900, Brazil
jorgehs@pucrs.br

Abstract. *In the present work the development of two-dimensional secondary instabilities in the baroclinic layer of a stably stratified temporal mixing layer is numerically investigated. The baroclinic layer is formed under the action of buoyancy effects and strains between the primary billows of the Kelvin-Helmholtz (K-H). When the fluid is strongly stratified and for higher Reynolds number this baroclinic layer may be subjected to secondary instabilities. Two different secondary instabilities are eventually found to develop upon the baroclinic layer: one originates near in the core regions of the K-H vortex and propagates towards the baroclinic layer, and another one of K-H type in the baroclinic layer itself. The occurrence of the secondary instabilities in the baroclinic layer is clearly shown using direct numerical simulation (DNS) of the Navier- Stokes equations in the Boussinesq approximation. Tests were done with Richardson numbers (*$Ri = 0;\ 0.07;\ 0.167$*) and Reynolds numbers (*$Re = 400;\ 500;\ 2000$*). The secondary instability of Kelvin-Helmholtz type was identified for Re from* 500 *when there is pairing process of the simulated vortices, and for* $Re = 2000$ *when only one vortex is simulated. In the simulation for* $Re = 500$*, the secondary K-H instability appears either* $Ri = 0.07$ *(weak stratification) as for* $Ri = 0.167$ *(strong stratification). This fact is not found in the current literature for a stably stratified mixing layer.*

keywords: *Secondary instability, baroclinic layer, Kelvin-Helmholtz, stably stratified, direct numerical simulation*

1. Introduction

The transition to turbulence in a stably stratified flow is a complex process with great importance for geophysical flows and engineering. The competition between the buoyancy and inertial forces modifies the dynamics of the stratified flow and alters the kind of instability that can be developed in it. The evolution of such flows is commonly studied in terms of a model problem: the mixing layer. The stably stratified mixing layer develops at the interface of two parallel streams of fluid moving horizontally at different velocities and with different densities, the upper stream being lighter than the lower one.

Miles (1961) and Howard (1961), based on a linear stability analysis, showed that for the occurrence of a Kelvin-Helmholtz (K-H) instability in stratified mixing layer from an infinitely small disturbance, the Richardson number should be less than 0.25 somewhere within the flow. This first instability that occurs in the mixing layer is due to the inflectional nature of the velocity profile (Michalke, 1964): the vortex sheet initially created is linearly unstable and rolls up to form the primary billows of K-H.

In the stably stratified mixing layer occurs a streamwise density gradient $(\partial\rho/\partial x)$ between the K-H vortices (in the braids). This streamwise density gradient, that corresponds to the spanwise component of the baroclinic torque in the Boussinesq approximation, feeds the braid with vorticity and forms thin vorticity layers there. The vorticity layers, that is formed under the action of the buoyancy effects and strains between the billows of the K-H, was defined as a baroclinic layer by Staquet (1995) and identified by Caulfield and Peltier, (2000). This streamwise density gradient develops in the braid and induces a secondary shear instability, which concentrates the vorticity in the baroclinic layer. Thus, the density gradient source term contributes as an extra mechanism

for the generation or destruction of local vorticity, by means of the baroclinic torque.

For the reason mentioned above the baroclinic layer does not exist in an unstratified flow. This baroclinic layer may be subjected to secondary instabilities when the fluid is strongly stratified and for higher Reynolds numbers. Evidences of occurrence of secondary instabilities in a baroclinic layer were reported in geophysical flows for the atmosphere (Gossard et al., 1970) and in the ocean (Haury et al., 1979), in a very few laboratory experiments (Atsavapranee and Gharib, 1997; Thorpe, 1985) and through numerical simulation (Staquet, 1995; Staquet, 2000; Smyth, 2003).

A theoretical model based on the similarity theory for braids to explain the dynamics of the baroclinic layer was developed by Corcos and Sherman, 1976. This model predicts that the Richardson number, which characterizes the stability of the braids, would be inversely proportional to the square root of the Reynolds number of the original shear layer. Consequently, to sufficiently high Reynolds numbers the necessary condition for the mixing layer instability, in the accord with the Miles-Howard theorem (Miles, 1961; Howard, 1961, $Ri \leq 0.25$), could be satisfied.

Staquet (1995) confirmed the validation of Corcos and Shermans theory (Corcos and Sherman, 1976) for the braids and successfully detected the secondary K-H instability in the baroclinic layer. A new mode of instability that is originated in the core regions and propagates to the braid, called near-core instability, was also identified.

Smyth (2003) extended the results of Staquet paper's to lower values of Richardson number ($0.04 \leq Ri \leq 0.16$), higher Prandtl numbers ($1 \leq Pr \leq 7$), and $Re \geq 1000$ in an unstable stratified mixing layer with a reference system attached to the braid (as in Corcos and Sherman, 1976). It was evidenced that the secondary K-H instability appears in the baroclinic layer when the Reynolds number exceeds ~ 1000, but it does not show the near-core instability.

The main objective of this work is to investigate the occurrence of the two-dimensional secondary instabilities in the baroclinic layer of a stably stratified mixing layer. In this study the development of the secondary instability in the baroclinic layer is clearly shown using direct numerical simulation (DNS). The DNS technique is used to solve the complete Navier-Stokes equations, in the Boussinesq approximation. The set of simulations includes runs with different Richardson numbers and different Reynolds number.

2. Secondary instabilities in a baroclinic layer

Two different secondary instabilities are found in the baroclinic layer: one is originated near-core of the K-H vortex (near-core instability) and propagates towards the baroclinic layer, and another one of Kelvin-Helmholtz type in the baroclinic layer. The development of these instabilities in the baroclinic layer depends on the stratification degree of the flow (Ri), on the Reynolds number and on the imposed initial conditions.

The near-core instability, as Staquet (1995) refers to, is developed near the unstable regions of the primary K-H vortex. The formation of a strong jet made by the baroclinic layer and adjacent vorticity layer of opposite sign created baroclinically by convective motions inside the primary K-H vortex is necessary to the amplification of the near-core instability. The near-core instability amplifies while it moves along the baroclinic layer towards the stagnation point region. Thus, it disturbes the flow field inducing a secondary instability of the Kelvin-Helmholtz type. This instability is developed in the baroclinic layer when the strain field acting over the layer is weakened and the stratification is strong. The result structures of the secondary K-H instability are very similar, in appearance and dynamics, to primary vortices of the K-H.

Figure 1 shows a schema of this physical phenomenon, where the positive vorticity (clockwise) correspond to the red color and the negative vorticity (counter-clockwise) corresponds to the blue color in the picture.

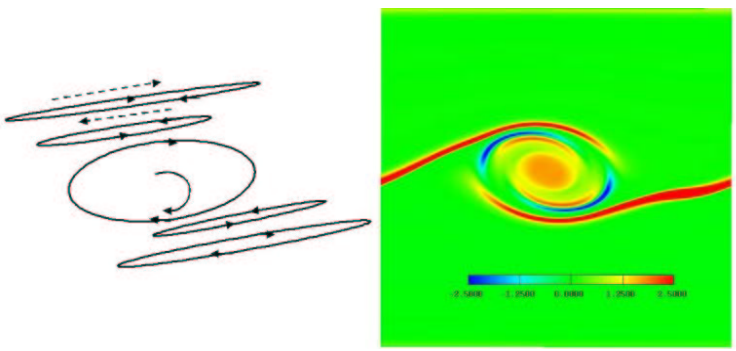

Figure 1: Schematic view of the near-core instability.

The numerical simulations of Staquet (1995) showed that when only one vortex is simulated and for Re values between 400 and 1000 the secondary near-core instability do not developed, possibly because the vorticity of the baroclinic layer and the adjacent layer of negative vorticity are weak for such development. For this range of the

Reynolds number the flow is stable to the secondary K-H instability in the baroclinic layer. On the other hand, for $Re > 400$ and $Ri = 0.167$ and two K-H vortices are simulated the secondary instabilities develop if pairing process is present. For $Re \geq 2000$ both instabilities occur in the flow, even if a vortex is simulated (Staquet, 1995). The present study is proved that secondary instabilities in the baroclinic layer occur for $Re \geq 500$ and $Ri = 0.07$, $Ri = 0.167$ when two K-H vortices are simulated and a subharmonic perturbation is added.

3. Mathematical model and numerical method

The temporal mixing layer with periodic conditions in the x-direction, and free-slip boundary condition in the z-direction is considered. We assume that the fluid motion is described by the Navier-Stokes equations using the Boussinesq approximation, in a Cartesian frame of reference $\Re = (0; x, z)$,

$$\frac{\partial \vec{u}}{\partial t} = -\nabla P - \vec{\omega} \times \vec{u} - Ri\ \rho\ \vec{i_z} + \frac{1}{Re}\nabla^2 \vec{u} \tag{1}$$

$$\frac{\partial \rho}{\partial t} + \vec{u} \cdot \nabla \rho = \frac{1}{RePr}\nabla^2 \rho \tag{2}$$

$$\nabla \cdot \vec{u} = 0 \tag{3}$$

where $\rho(x, z, t)$ is density or active scalar, $\vec{u}(x, z, t)$ is the velocity field, $P(x, z, t)$ is the modified pressure field and $\vec{\omega}$ is the vorticity field. There are two non-dimensional relevant parameters; the Reynolds number $Re = U\delta_i/\nu$ (based on the half velocity difference across the shear layer and on the initial vorticity thickness, defined by $\delta_i = 2U/(du/dz)_{max}$) and the Richardson number $Ri = g\Delta\rho R\delta_i/\rho_0 U^2$ (where $\Delta\rho R$ is density scale and R is the ratio of initial vorticity thickness to the density thickness). Here the thickness of the initial velocity profile is approximately 80% of the thickness of the initial density profile. The time is made dimensionless using the advective scale δ_i/U. We chose the units of length, velocity and density such that $\delta_i = 1$, $U = 1$ and $\Delta\rho = 1/R$. In this manner, $Re = 1/\nu$ and $Ri = g/\rho_0$. At $t = 0$, $\rho(x, z, t) = \rho_0 + \rho(z)$, where ρ_0 is a constant density reference and $\rho(z)$ is the basic density profile. In the present case, no density fluctuation is superposed upon $\rho(z)$ at $t = 0$. The initial profiles of velocity and density are

$$u(z, t = 0) = U\mathrm{erf}\Big(\tfrac{\sqrt{\pi}z}{\delta_i}\Big) \tag{4}$$

$$\rho(z, t = 0) = -\frac{1}{R}\mathrm{erf}\Big(\tfrac{\sqrt{\pi}Rz}{\delta_i}\Big)\,. \tag{5}$$

A two-dimensional sinusoidal perturbations is superimposed upon the basic velocity profile. This perturbation is composed by two waves corresponding to the most amplified wave number α_a and its firth sub-harmonic $\alpha_a/2$. The associated most unstable wavelength given by linear stability theory is approximately $\lambda_a = 7\delta_i$ (the most amplified wave number $\alpha_a = 2\pi/\lambda_a$ being $0.889\delta_1^-1$ (Michalke, 1964)). These perturbations promote, respectively, the development of the Kelvin-Helmholtz instability and vortex pairing. In such case, the side of computational domain is taken equal to $L_x = 7N\delta_i$ in order to obtain N vortices in the streamwise direction.

Equations (1-3) are solved numerically using a sixth-order compact finite difference scheme (Lele, 1992) to compute the spatial derivatives, while the integration is performed with a third-order low-storage Runge-Kutta method (Williamson, 1980). The incompressibility condition, Eq.(3, is ensured with a fractional step method via resolution of Poisson equation for the pressure. The evolution of a small sinusoidal disturbance was considered to validate the numerical code, and results were compared with linear stability theory (Martinez et al., 2004). More details about the numerical code can be found in Lardeau et al., 2002 and Silvestrini and Lamballais, 2002.

4. Results

4.1. Physical and numerical parameters of the simulations

The parameters are summarized in Tab.1. The amplitude of the perturbation superimposed upon the basic velocity profile, for the fundamental and the subharmonic mode, is showed in of the Tab. 1.

4.2. Development of secondary instabilities in the baroclinic layer

In previous simulations, at $Re = 300$, the formation of the baroclinic layer was observed, but without manifestation of secondary Kelvin-Helmholtz instability (Martinez et al., 2004). In the test made at $Re = 400$ and $Ri = 0.167$, where only one vortex is simulated, it was possible to observe the formation of the baroclinic

Table 1: Physical and numerical parameters of the two-dimensional simulations.

Simulation	Re	R_i	Domain $L_x \times L_z$	Grid $n_x \times n_z$	Amplitude
$2DI$	400	0.167	$7\delta_i \times 7\delta_i$	256×257	$(1\%U; 0)$
$2DII$	2000	0.167	$7\delta_i \times 7\delta_i$	768×961	$(1\%U; 0)$
$2DIII$	500	0.07	$14\delta_i \times 14\delta_i$	512×513	$(1\%U;\ 0.1\%U)$
$2DIV$	500	0.167	$14\delta_i \times 14\delta_i$	512×513	$(1\%U;\ 0.1\%U)$
$2DV$	2000	0	$14\delta_i \times 14\delta_i$	768×961	$(1\%U;\ 0.1\%U)$
$2DVI$	2000	0.07	$14\delta_i \times 14\delta_i$	768×961	$(1\%U;\ 0.1\%U)$
$2DVII$	2000	0.167	$14\delta_i \times 14\delta_i$	768×961	$(1\%U;\ 0.1\%U)$

layer. This simulation, the K-H vortex reaches the maximum amplitude and satures at time $t = 39.6\delta_i/U$ (Caulfield and Peltier, 2000). This fact occurs without presenting instabilities in the baroclinic layer, Fig. 2, what is in accordance with the work of Staquet (1995).

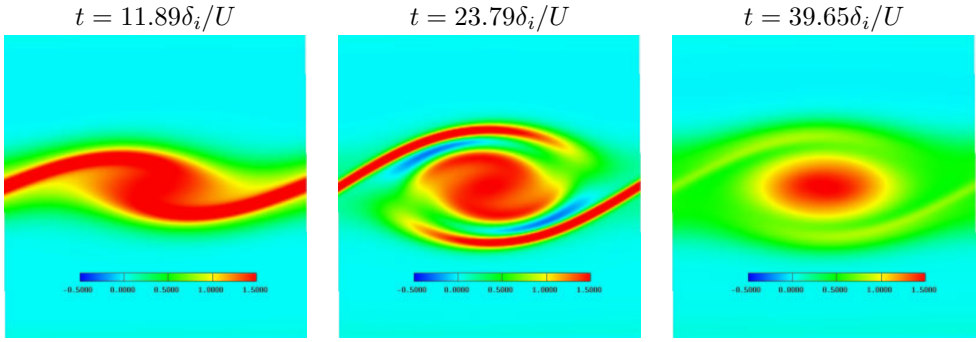

Figure 2: Spanwise vorticity field (ω_y). Simulation $2DI$, $Re = 400$, $R_i = 0.167$.

In the results of Staquet (1995) was identified the secondary K-H instability, without the formation of the near-core instability, at $Re = 400$ and $Ri = 0.167$ with a computational grid of $n_x \times n_y = 512, 257$ points and domain of $(L_x, L_y) = (14\delta_i, 7\delta_i)$. Smyth (2003) does simulations using an unstable density profile for $Re = 1000$ and $Ri = 0.08$, and for $Re \geq 2000$ with different Richardson numbers. It was identified the secondary K-H instability in all simulations, except in the $Ri = 0.04$ and $Re = 2000$ simulation.

In this work, the secondary K-H instability is identified for Reynolds number from 500 when there is a pairing of the simulated vortices and for $Re = 2000$ when only one vortex is simulated (Fig. 3). In the simulation $2DIII$ and $2DIV$, at $Re = 500$, the secondary K-H instability appears for $Ri = 0.07$ and for $Ri = 0.167$ (Fig. 4 e 5). This fact is not found in the stratified mixing layer reported in the literature.

In test $2DII$, at $Re = 2000$ and $R_i = 0.167$, with a vortex, the formation of a near-core instability is observed, which is amplified towards the baroclinic layer and unstables it. This process provokes the appearance of a new secondary K-H instability, forming small vortices in the baroclinic layer (Fig. 3). The secondary near-core instability , as it was reported before, appears due to the formation of a negative vorticity layer (blue color) generated between two co-rotating vortices, formed by baroclinic layer of positive vorticity (red color) and the core of the primary K-H vortex, by the strong streamwise density gradient. The negative vorticity layer unstables the baroclinic layer and makes it become a similar to shear layer. The new mixing layer, when unstable, forms small vortices of the K-H type with the same dynamics as the primary K-H vortices.

Figures 4 and 5 show that the pairing process occurs at the times $t = 37.69\delta_i/U$ and $t = 43.64\delta_i/U$ for the case at $R_i = 0.07$ and $R_i = 0.167$, respectively, and the baroclinic layer is well visible. After the pairing a vorticity of opposite sign to the flow (in blue) around the new vortex comes up. This negative vorticity next to vortex creates a jet that unstables the baroclinic layer as a consequence a new vortex is stretched between the negative vorticity layers. The baroclinic layer turned unstable, presenting the secondary K-H instability, shows K-H vortices pairs of oppositive sign.

The negative vorticity is formed baroclinically when heavy (or light) fluid completes a first revolution inside the primary K-H vortex. Such convective motion reinforces locally streamwise density gradients due to the overlapping of light fluid layers among heavy fluid (gravitational convective instability). In the test with $R_i = 0.07$ the vorticity decreases and saturates.

In the Fig. 6a it can be observed the temporal development of the maximum and minimum vorticities for

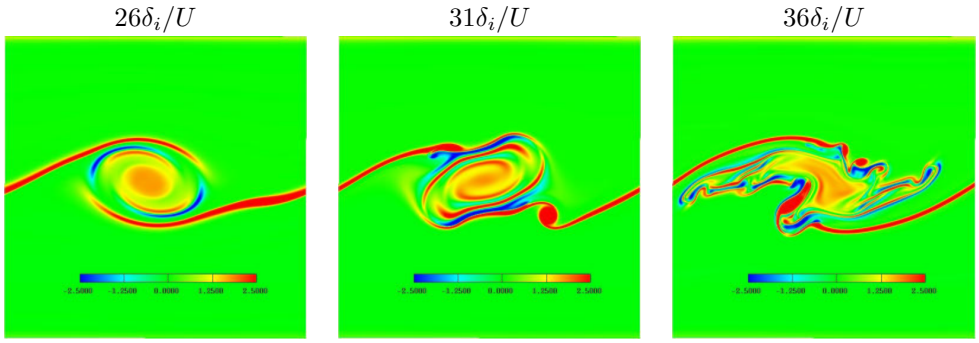

Figure 3: Development of secondary instabilities in the baroclinic layer. Spanwise vorticity field (ω_y). Simulation $2DII$, $Re = 2000$,$R_i = 0.167$.

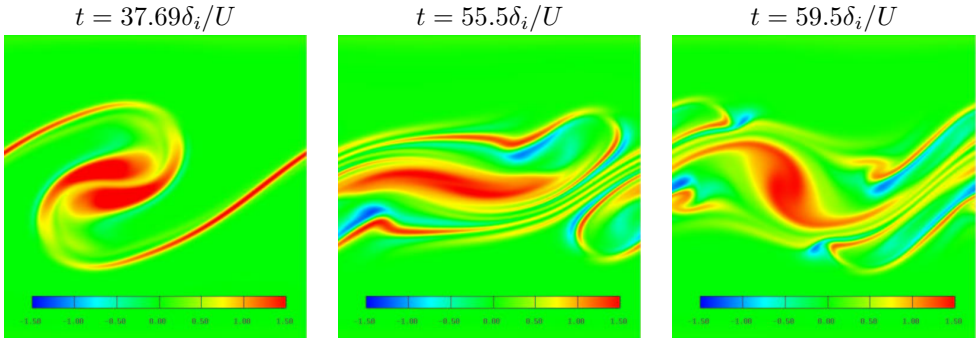

Figure 4: Development of secondary instabilities in the baroclinic layer. Spanwise vorticity field (ω_y). Simulation $2DIII$, $Re = 500$, $R_i = 0.07$.

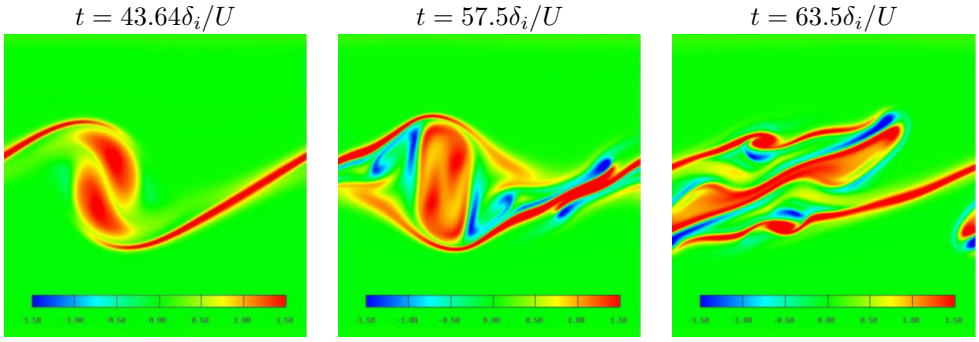

Figure 5: Development of secondary instabilities in the baroclinic layer. Spanwise vorticity field (ω_y). Simulation $2DIV$, $Re = 500$, $R_i = 0.167$.

simulations $2DIII$ and $2DIV$. It can be noticed that the vorticity at $R_i = 0.167$ increases beyond the initial value and that simultaneously a negative vorticity decrease. In the case at $Ri = 0.07$ the negative vorticity moves away from zero, what was not observed in the simulations at $Re = 300$ (Martinez et al., 2004), where the secondary K-H instability did not propagate. It demonstrates that the production of negative vorticity inside the vortex core is rapidly followed by the growth of the secondary K-H instability. This instability does not develop if the negative vorticity is too low compared to the positive one. It can be said that the Reynolds number, along with the Richardson number, has strong influence in the development of this kind of instability.

Figure 6b shows the spectrum of kinetic energy in function of the streamwise wave number at different times, referring simulation $2DIV$, $Ri = 0.167$. This spectrum suggests a mechanism of transference of energy towards dissipative scales, through a "cascade" of self-similar Kelvin-Helmholtz instabilities. Such a mechanism could contribute to mixing at small scales in geophysical flows.

Figure 7 shows that without stratification the formation of the secondary K-H instability can not be possible, and obviously there is not formation of the baroclinic layer. In this work it was verified that the secondary K-H instability is not developed in the baroclinic layer if the negative vorticity is quite next to zero, as it happens when the flow is homogeneous ($R_i = 0.0$).

The vorticity increase can be verified in Fig. 8, where the temporal evolution of the maximum and minimum

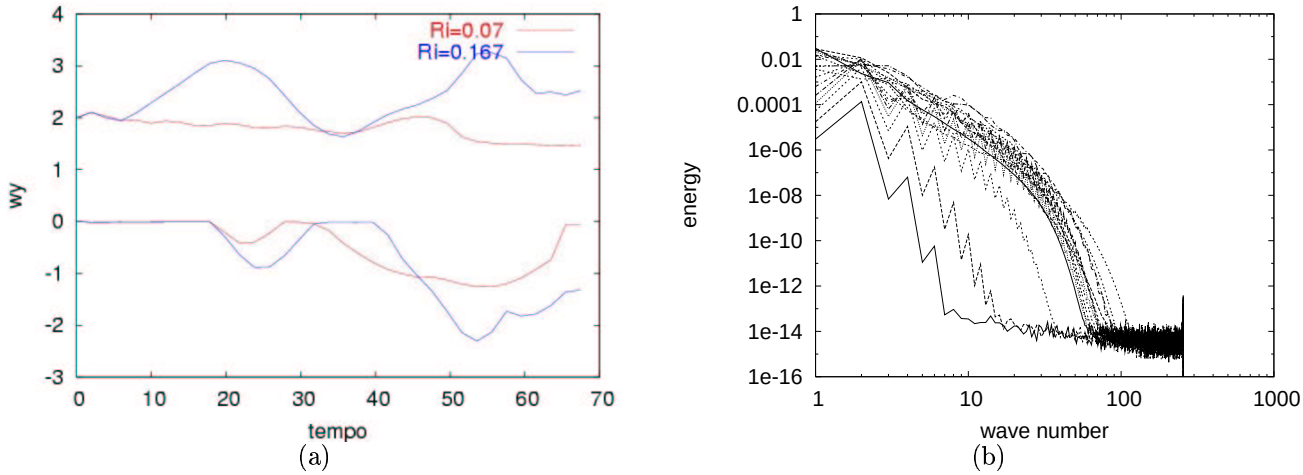

Figure 6: (a)Temporal evolution of the maximum and minimum vorticity (ω_y). For $R_i = 0.07$ and $R_i = 0.167$, simulation $2DIII$ and $2DIV$, respectively. (b)Spectrum of kinetic energy in function of the streamwise wave number at different times and $R_i = 0.167$, simulation $2DIV$

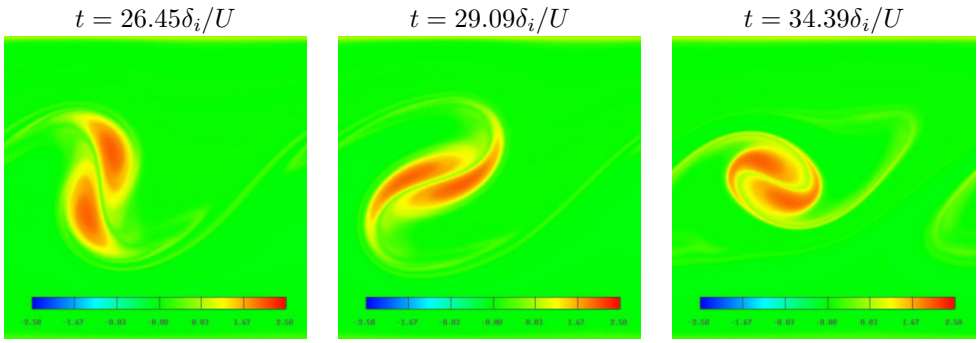

Figure 7: Spanwise vorticity field (ω_y). Simulation $2DV$, $Re = 2000$, $R_i = 0.0$.

vorticity (ω_y) is shown, for Richardson numbers 0; 0.07 and 0.167 and $Re = 2000$. It is the non-conservation of the local vorticity that makes possible the successive secondary instabilities displayed, permitting the existence of a baroclinic layer of higher vorticity than the maximum initial vorticity, as well as the generation of the negative vorticity.

In Figure 9, it is observed that after the pairing a negative vorticity (in blue) appears between the vortex and the baroclinic layer. Even if it is not so strong as to $Ri = 0.167$ (Fig. 10), the negative vorticity amplifies until the point that it disturbs the baroclinic layer and induces the secondary K-H instability in it. This fact is not shown in the literature (Staquet, 1995). where the simulations are made at $Ri = 0.167$ and for different Reynolds numbers.

When $Re = 2000$ and $R_i = 0.167$ it is verified that vorticity increase beyond its maximum initial value $(2U/\delta_i)$(due to the generation of vorticity by the spanwise component of the baroclinic torque), both instabilities are showed (see Fig. 10).

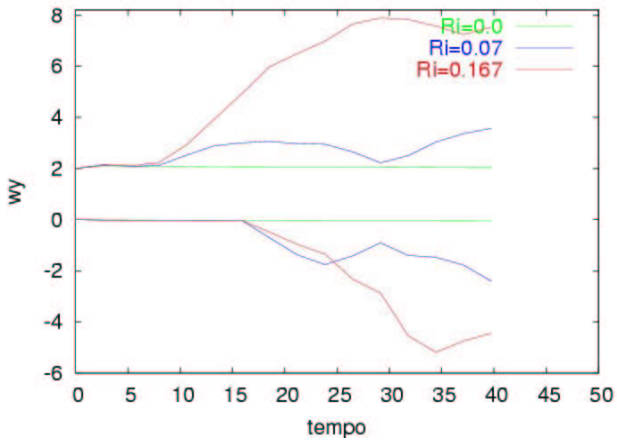

Figure 8: Temporal evolution of the maximum and minimum vorticity (ω_y), for $R_i = 0$, $R_i = 0.07$ and $R_i = 0.167$; Simulation $2DV$, $2DVI$ and $2DVII$, respectively.

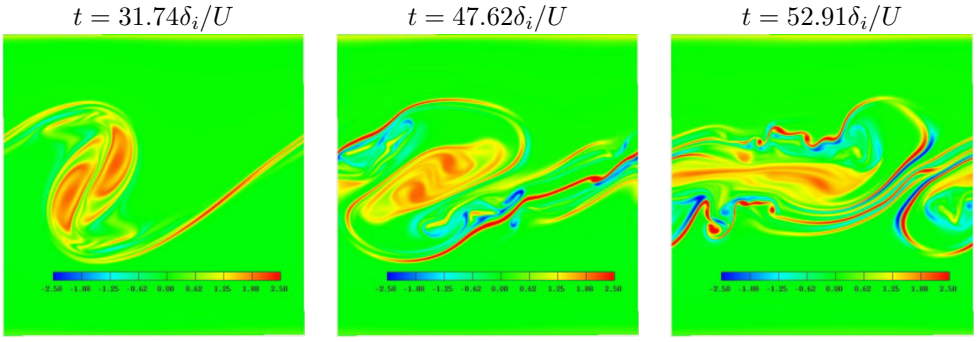

Figure 9: Development of secondary instabilities in the baroclinic layer. Spanwise vorticity field (ω_y). Simulation $2DVI$, $Re = 2000$,$R_i = 0.07$.

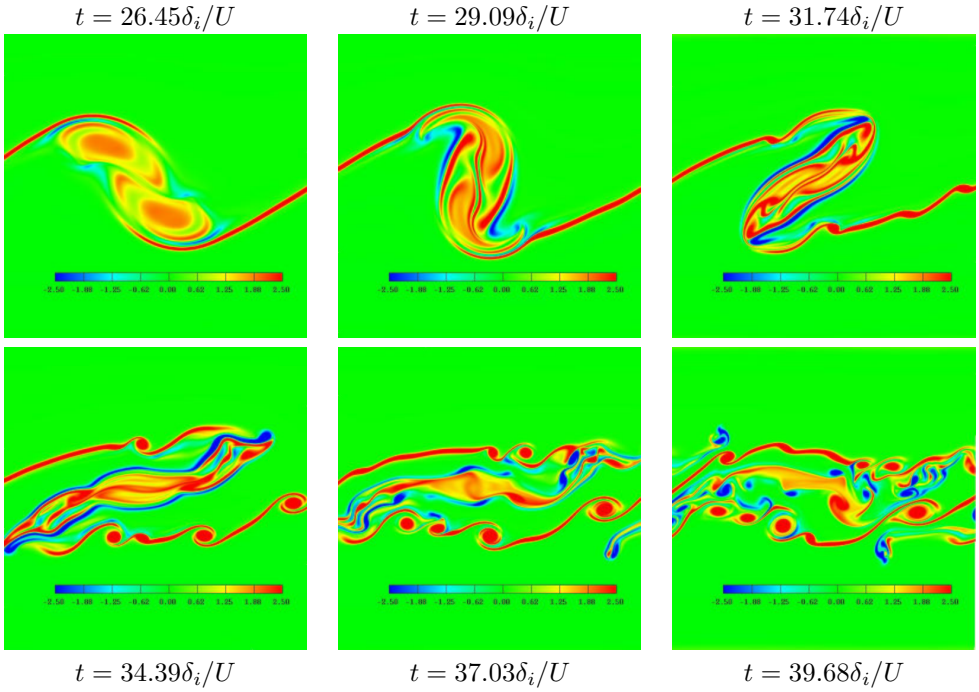

Figure 10: Development of secondary instabilities in the baroclinic layer. Spanwise vorticity field (ω_y). Simulation $2DVII$, $Re = 2000$, $R_i = 0.167$.

5. Conclusion

The purpose of the present study was to investigate numerically the occurrence of the two-dimensional secondary instabilities in the baroclinic layer of a stably stratified mixing layer. The occurrence of the secondary

instability in the baroclinic layer was clearly demonstrated using direct numerical simulation. It was verified that in the baroclinic layer two different secondary instabilities under development can be found: one is originated near-core of the K-H vortex and propagates towards the baroclinic layer, and another one of Kelvin-Helmholtz type in the baroclinic layer. Also, it was verified that a necessary condition for near-core instability to amplify seems to be the formation of a strong jet made by the baroclinic layer and by an adjacent vorticity layer of opposite sign created baroclinically by convective motions inside the primary K-H vortex.

The secondary Kelvin-Helmholtz instability and near-core instability were identified at Reynolds number from 500 when a pairing of the simulated vortices occurred and at $Re = 2000$ when only one vortex was simulated. In the simulation at $Re = 500$, the secondary instabilities appeared both at $Ri = 0.07$ (weak stratification) and at $Ri = 0.167$ (strong stratification). The same happened in the simulation at $Re = 2000$ and $Ri = 0.07$. This fact is not reported in the literature, where the simulations were made at $Ri = 0.167$ and at different Reynolds numbers. An earlier near-core instability amplifies for $Ri = 0.167$ and $Re \geq 500$ in the baroclinic layer, is identified if the negative vorticity layer of magnitude is comparable with the positive vorticity.

We can conclude, based on the simulations presented in this work, that the calculation code employed solves the small scales and instabilities found in the baroclinic layer and that the resolution of the computational grids was chosen in agreement. However, the following doubt comes up: How do the two-dimensional secondary instabilities demonstrated above compete with the three-dimensional instabilities?

6. Acknowledgements

The first author acknowledge the financial support received from CAPES-PICDT.

7. References

Atsavapranee, P. and Gharib, M., 1997, Structures in stratified plane mixing layers and the effects of cross-shear, "J. Fluid Mech.", Vol. **342**, pp. 53–86.

Caulfield, C. P. and Peltier, W. R., 2000, The anatomy of the mixing transition in homogenuos and stratified free shear layers, "J. Fluid Mech.", Vol. **413**, pp. 1–47.

Corcos, G. M. and Sherman, F. S., 1976, Vorticity concentration and the dynamics of unstable free shear layers, "J. Fluid Mech.", Vol. **73**, part2, pp. 241–264.

Gossard, E. E., Richter, J. H., and Atlas, D., 1970, Internal waves in the atmosphere from high-resolution radar measurements, "J. Geophys. Res.", Vol. **75**, pp. 3523–3535.

Haury, L. R., Briscoe, M. G., and Orr, M. H., 1979, Tidally generated internal wave packets in Massachusetts Bay, "Nature", Vol. **278**, pp. 312–317.

Howard, L. N., 1961, Note on a paper of John W. Miles, "J. Fluid Mech.", Vol. **10**, pp. 509–512.

Lardeau, S., Lamballais, E., and Bonnet, J. P., 2002, Direct Numerical Simulations of a jet controlled by fluid injection, "J. Turbulence", Vol. **3 (002)**, pp. –.

Lele, S. K., 1992, Compact finite difference schemes with spectral-like resolution, "J. Comp. Phys.", Vol. **103**, pp. 16–42.

Martinez, D. M. V., Schettini, E. B. C., and Silvestrini, J. H., 2004, Transition to turbulence in a stable stratified temporal mixing layer through direct numerical simulation, "Proceedings of the 10th Congress of Thermal Sciences and Engineering", p. 11, Rio de Janeiro, RJ, Brazil.

Michalke, A., 1964, On the inviscid instability of the hyberbolic tangent velocity profile, "J. Fluid Mech.", Vol. **19**, pp. 543–556.

Miles, J. W., 1961, On the stability of heterogeneous shear flows, "J. Fluid Mech.", Vol. **10**, pp. 496–508.

Silvestrini, J. H. and Lamballais, E., 2002, Direct Numerical Simulations of wakes with virtual cylinders, "Int. J. Comp. Fluid Dyn.", Vol. **16 (4)**, pp. 305–314.

Smyth, W. D., 2003, Secondary Kelvin-Helmholtz instability in weakly stratified shear flow, "J. Fluid Mech.", Vol. **497**, pp. 67–98.

Staquet, C., 1995, Two-dimensional secondary instabilities in a strongly stratified shear layer, "J. Fluid Mech.", Vol. **296**, pp. 73–126.

Staquet, C., 2000, Mixing in a stably stratified shearlayer: two and three-dimensional numerical experiments, "Fluid Dynamics Research", Vol. **27**, pp. 367–404.

Thorpe, A., 1985, Laboratory observations of secondary strutures in Kelvin-Helmholtz billows and consequences for ocean mixing, "Geophys. Astrophys. Fluid Dyn.", Vol. **34**, pp. 175–199.

Williamson, J. H., 1980, Low-storage Runge-Kutta schemes, "J. Comp. Phys.", Vol. **35**, pp. 48.